EARTH PRP-011

Update status EARTH November 2014

14 November 2014

R.J. de Meijer, M. Reuver, M.W. van Rooy, S.W. Steyn and W. van Westrenen

Stichting Earth AntineutRino TomograpHy (EARTH)
de Weehorst
9321 XS Peize, The Netherlands
www.geoneutrino.nl

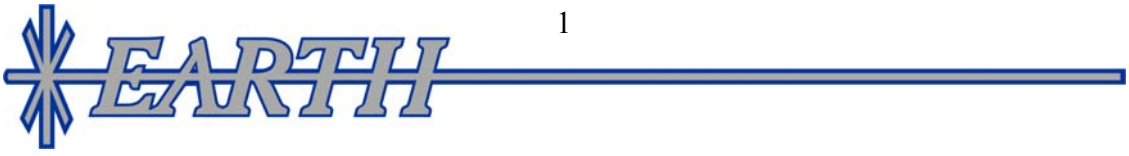

Preface

1. Introduction.

This report presents the progress of the EARTH programme since the last report, published in August 2012. An earlier report, EARTH PRP-007, published in July 2009 gave a comprehensive overview of the project and the reader is referred to EARTH PRP-007 for further details and background information.

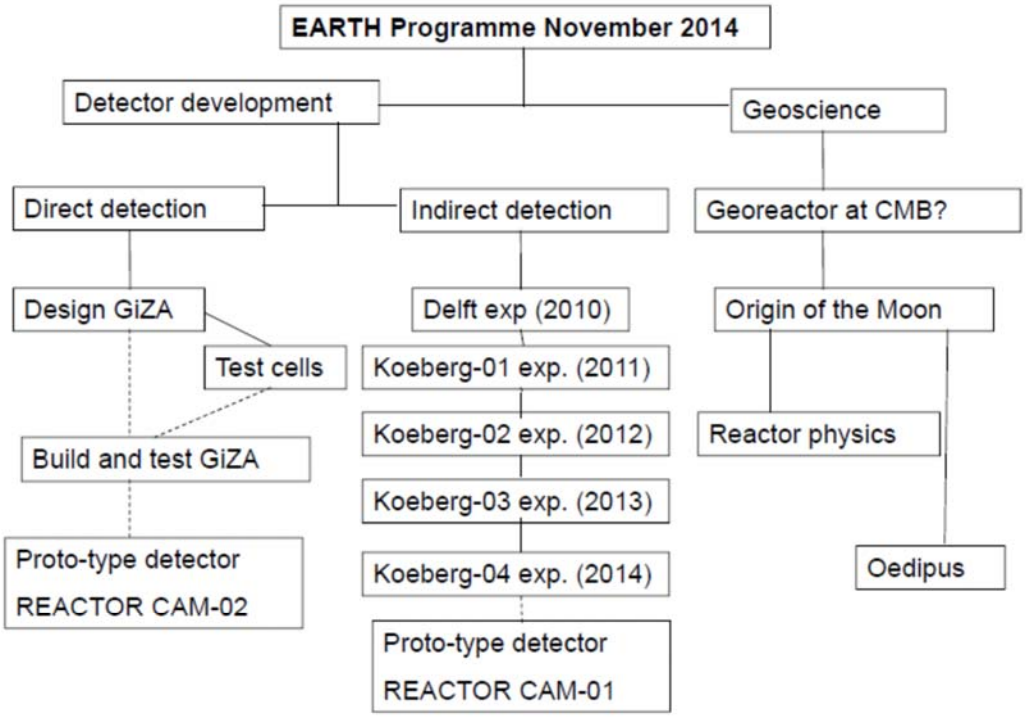

Figure 1. Schematic overview of various activities within the EARTH programme as at November 2014. The solid connecting lines indicate past and ongoing activities while the dashed lines are projections into the future.

The present and planned activities within the EARTH programme have schematically been presented in Fig. 1. The solid lines indicate the parts of the programme, being either completed or in progress. The programme has two main activities: Antineutrino detector development and Geoscience aspects that could result from the eventual data collection of antineutrinos emitted by various radiogenic processes in Earth. The present update will be structured according to this scheme.

2. Detector development.

The preferred detection mechanism for antineutrinos depends on its energy. For energies above approximately 10 MeV Cherenkov radiation provides a direct way of antineutrino

detection in which energy and incoming direction can be deduced. For low-energy (<~10 MeV) antineutrinos Cherenkov radiation is not sensitive enough anymore and the most common detection is the so-called inverse beta-decay reaction in which the antineutrino is captured on a free proton and subsequently a positron and a neutron are emitted.

The event is detected via the annihilation of the positron in which it combines with an electron and subsequently two annihilation quanta, each with an energy of E=511keV, are emitted. The neutron is detected after it has been captured by a nucleus. Commonly the capturing nucleus is H in liquid scintillators or plastic often doped with Gd (Gadolinium). In both the annihilation and the capture on H and Gd γ-radiation is emitted.

Detector systems based on this detection mechanism have been demonstrated near nuclear power reactors at Rovno, Songs and Osiris. These detectors have in common that they are quite large in size and weight due to a combination of reasons:

- The low cross section for the capture process;
- A threshold energy of 1.8 MeV, excluding the majority of the antineutrinos released in the fission process inside the reactor;
- The long range (~30-50cm) of γ-radiation in the detection material; and
- The large amount of shielding against cosmic muons and environmental radiation.

Some reduction in size and weight may be achieved by detecting the outgoing particles in another way than by γ-radiation. This is the approach that we have taken in the development of the GiZA detector as indicated in figure 1 as Direct detection. It allows for a more compact detector, but is still limited by the low cross section and the threshold energy.

The antineutrino energy region below 1.8 MeV has hardly been explored. It requires an interaction of antineutrinos with a radionucleus emitting β^+ radiation. For this reaction one assumes antineutrino interaction with a bound proton leading to β^+ radiation and a neutron bound inside the nucleus. Being unstable to β^+ radiation implies that there is no threshold and the positron even has surplus energy. In the β^+ decay the final nucleus is often left in an excited state, rapidly decaying by emission of γ-radiation. The antineutrino is detected indirectly by an process affecting the β^+ decay.

Rather than a large volume in which the reaction takes places and the produced radiation is detected, we have a very compact system with a small sized source about 10 mm^3 surrounded by a dense material selected for γ-radiation. At present we focus on this process indicated in figure 1 by Indirect detection. The progress is described in section 2.2.

2.1 Direct detection of antineutrinos

The activities in this development were shelved for the time being because of the activities in the indirect detection measurements.

2.2 Indirect detection of antineutrinos.

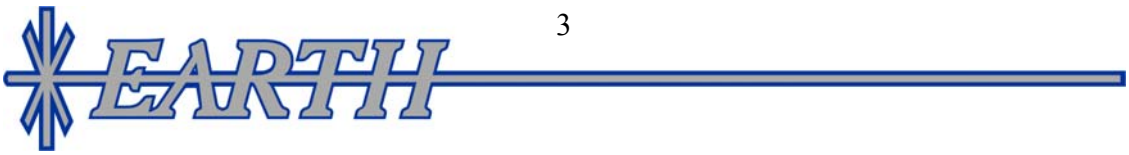

2.2.1 Koeberg-03 measurements

In the previous progress report (EARTH PRP-10) we presented an overview of the measurements at Delft (*de Meijer et al., 2011*) and at the Koeberg nuclear power station (Koeberg-01 and Koeberg-02). Both measurements at Koeberg were plagued by instrumental problems, making the outcome of the measurements unreliable, hence a third series of measurements was conducted at the seismic vault direct under unit#1 of Koeberg. The text and figures of this section of the report is to a large extent taken from a manuscript, recently submitted for publication. It presents the set-up and the results. For the analytical procedures and the assessment of the systematic uncertainties we refer to the forthcoming publication (*de Meijer and Steyn, 2014)*.

From the two previous measurements it became clear that a stable measurement environment is a prerequisite for long-term, high quality data. Moreover, from analysing the first two measurements it also became clear that coincident summing provides a way of experimentally separating events from the β^+-decay- and electron capture (EC) branches. Based on these experiences, the set-up was redesigned for optimum sensitivity for coincident summing and the compact hard- and software acquisition system. For the third series the detector used was a 10.4*10.4 cm cylindrical NaI well counter with a 12mm diameter, 51mm deep well in which the source can be placed. The detector was manufactured by SCIONIX–Holland B.V.. It plugged into an ITECH Venus base that incorporates all the necessary electronics and was connected to a laptop via the USB port. The on-line spectrum stabilisation and spectra storage was done by the INTERWINNER software provided with the Venus base. The detector and the PMT were housed inside a cylindrical lead shield with 7.5cm lead walls and an inner copper lining. At the top there are two 7.5cm thick, dove tailed sliding doors of lead; at the bottom there is an 85mm diameter hole through which the VENUS-base protruded. Directly below the bottom of the vertical lead cylinder, at a distance of about 20cm, there were two 5cm thick lead discs that provided shielding against radiation from the floor.

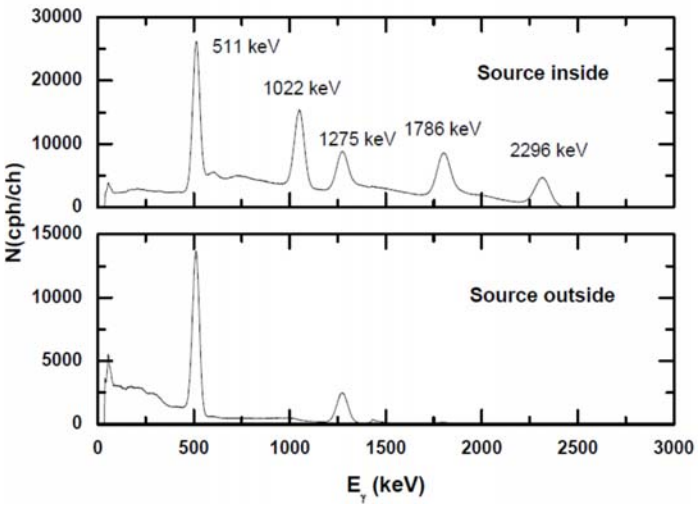

Figure 2. Gamma-ray spectra with a NaI well detector and the ^{22}Na source inside the well (top) and outside the detector (bottom).

The ^{22}Na source was glued into a Perspex holder then wrapped in a 1mm thick Al foil and surrounded by ~3mm Pb foil. The source strength was estimated to be ~2kBq from the count rate at the start of the measurements.

Shown in Fig. 2 are spectra taken with the source inside and outside the well of detector which illustrates the effect of coincident summing in reducing the low energy part of the spectrum and strengthening the high energy part of the spectrum. The bottom panel shows the "traditional" spectrum of ^{22}Na with the prominent 1275 and 511 keV peaks due to the de-excitation of the first excited state of ^{22}Ne and one of the quanta from the positron annihilation, respectively (see Fig. 3). With the source inside the detector, additional peaks show up at 1022 (2*511) keV, 1786 (1275+511) keV and at 2297 (1275+2*511) keV. Moreover one notices that the shape of the continuum part of the spectra has changed due to the summing effects. This change in continuum shape complicates the continuum estimate and hence makes the net peak count rates systematically less reliable. The comparison of the two spectra clearly indicates that all events (except for the background in this energy range) above the 1275 keV peak are due to coincident summing only and hence are exclusively related to β^+-decay.

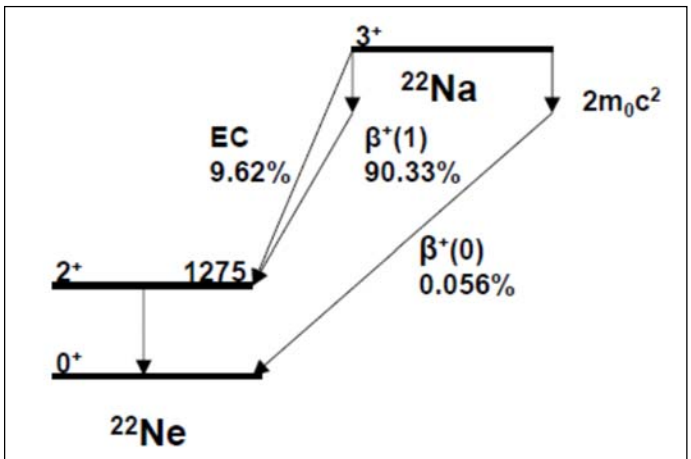

Figure 3. Decay scheme of ^{22}Na.

The measurements of this series cover two periods: 3 January-28 May 2013 and 20 August 2013-9 February 2014. During the first series a short BG measurement was conducted from 12 to 21 February. On 20 May a BG measurement was started, but on 28 May the system was inadvertently shut down and went unnoticed until 20 August. On 20 August 2013 a long background measurement run was started, which continued until 8 October, on which date a new series of Na+BG measurements was started that lasted until 9 February 2014.

The INTERWINNER software applies an online linear spectrum stabilisation. In these measurements a gate around the 1275 keV peak was used as the stabilisation point. A fine-gain adjustment was applied roughly every ten minutes. The adjustments were logged in a file for off-line assessment.

With the high count rate and the long measuring times a number of limitations in the data acquisition hard- and software showed up. Some of the limitations influenced the count rate but could be corrected for. Others restricted the selection of data for further analytical procedures. In the forthcoming publications these procedures and restrictions

are discussed and a due diligence cross check is made of the influence of these procedures on potential systematic uncertainties and errors.

In the analysis three Regions of Interests (RoI) in the energy spectrum (gates) have been selected: a total energy gate (169-2451 keV), a broad gate on the 1275 keV peak (1152-1353 keV) and Gate-I (1353-1921 keV). The analysis was carried out for a total of two ON-OFF-ON transitions of reactor unit#1: one in February-May 2013 and a second one in the period October 2013-February 2014. This resulted in the two data sets for Gate I (1353-1921 keV) and Gross 1275 keV (1152-1353 keV) plotted in Fig. 4. To reduce the statistical scatter of the results 7 day averages are plotted.

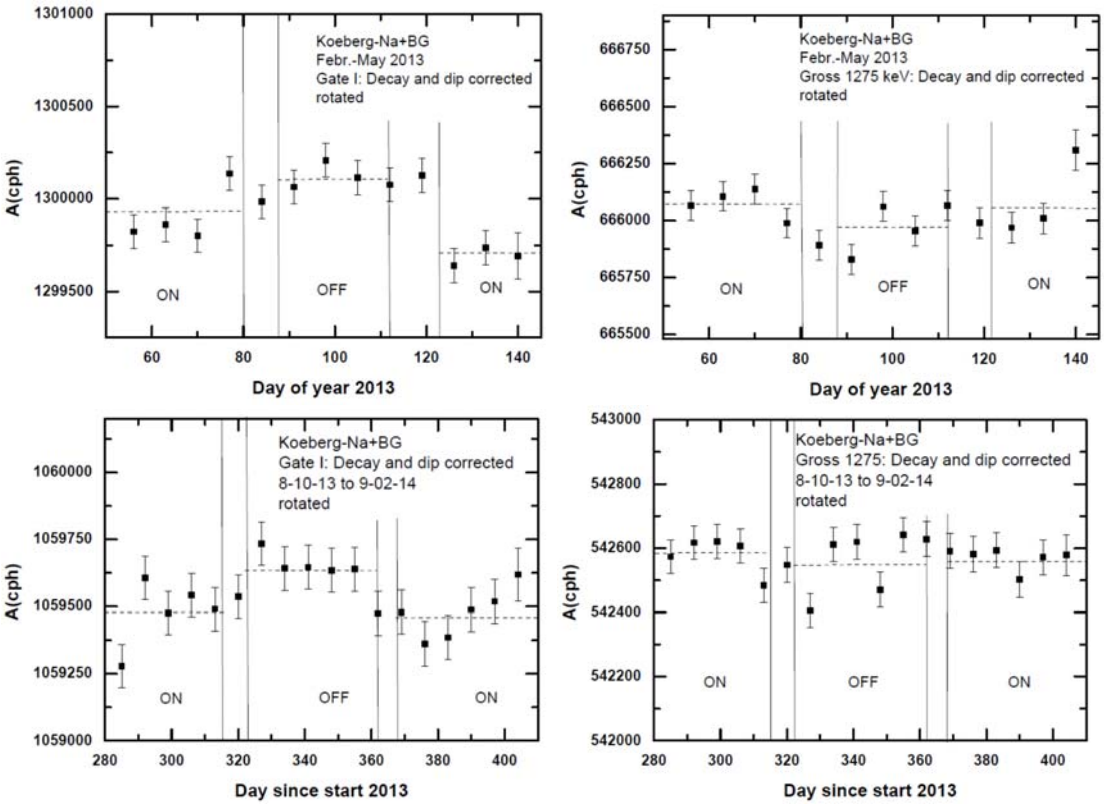

Figure 4. Count rates averaged over seven days for Gate I and Gate Gross 1275 keV. The vertical lines indicate the dates in which the transition from ON-OFF or vice versa occurred. The dash lines represent the weighted average for the period.

From the data plotted in Fig. 4 one notices that the count rates decrease for Gate-I during reactor-ON whereas the count rates increase in gate Gross 1275 keV during the same period. Of interest is to note that while the count rate in the Gross 1275 keV gate is affected by both β^+-decay and EC, whereas the count rate in Gate-I is affected by β^+-decay only. One needs to caution against labelling this a physics effect as instrumental effects may still play a roll.

The fact that the count-rate changes in the two gates as a function of reactor status have opposite signs for the E_γ =1152-1351 keV gate (Gross 1275 keV) and E_γ =1353-1921 keV gate (Gate-I) should have an effect on the count rate change for an almost total energy gate (E_γ =169-2451 keV). Due to the opposite effects in Gross 1275 keV and Gate I the effect should relatively be reduced. The count rates of Gate Total show a proper linear behaviour and hence may be analysed with the procedures described in *de Meijer and Steyn, 2014*. In Fig. 5 the count rate evolutions are presented for the periods February-May 2013 and October-February 2014. Both panels in the figure show a drop in

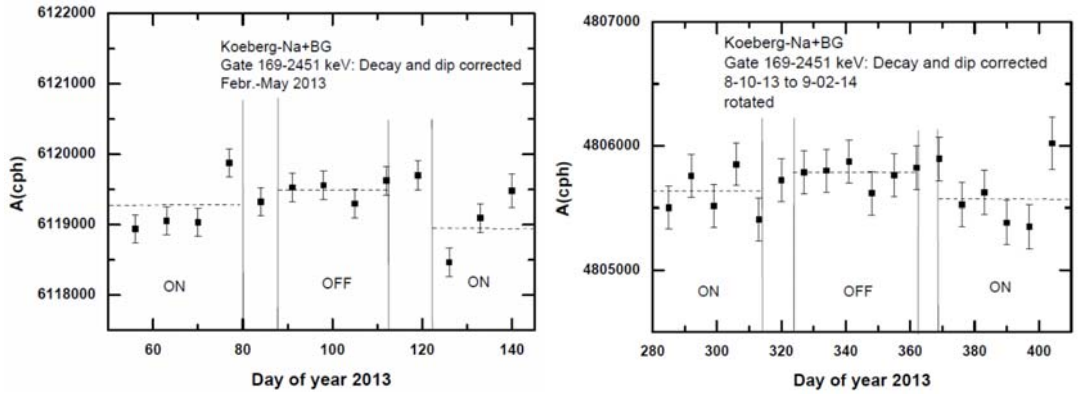

Figure 5. Count rates averaged over seven days for the energy gate E_γ =169-2451 keV. The vertical lines indicate the dates in which the transition from ON-OFF or vice versa occurred. The dash lines represent the weighted average for the period.

count rate during reactor-ON periods. Included in the E_γ =169-2451 keV gate are the two gates under discussion plus β^+-decay related events such as the 511 and 1022 keV peaks and their associated continua.

Table 1. Value of the weighted average count rate with corresponding χ2-values and the average difference between ON and OFF count rates.

DOY 2013	Status	A_{total} (cph) 169-2451 keV	χ^2	A_{1275} (cph) (1152-1353 keV)	χ^2	A_{Gate-I} (cph) (1353-1921 keV)	χ^2	$\left[\frac{\Delta A}{A_{OFF}}\right] * 10^4$ Total	$\left[\frac{\Delta A}{A_{OFF}}\right] * 10^4$ 1275	$\left[\frac{\Delta A}{A_{OFF}}\right] * 10^4$ Gate I
53-80	ON	6119280±110	1.41	666080±40	1.25	1299930±50	1.28			
87-112	OFF	6119490±100	1.11	665980±30	1.61	1300110±50	1.41	-0.66±0.16	1.4±0.5	-2.3±0.3
122-140	ON	6118950±110	1.79	666060±40	1.39	1299720±60	2.04			
								-0.52±0.11	***0.9±0.5***	***-1.9±0.4***
282-315	ON	4805640±80	1.02	542590±30	1.32	1059480±40	0.97			
323-362	OFF	4805287±70	1.21	542550±20	1.33	1059640±30	1.87	-0.39±0.16	0.4±0.5	-1.6±0.3
368-389	ON	4805070±80	1.27	542560±30	0.26	1059460±40	1.15			

Table 1 presents the weighted averages of the count rates during a full reactor-status period (ON or OFF) used in Fig. 4 and 5. Also tabulated is the average change of count rate during the two reactor-ON periods on either side of the reactor-OFF period, relative to the count rate during reactor-OFF period. The combined result of the two data sets is -0.52±0.11, +0.9±0.5 and -1.9±0.4, for Total, Gross 1275 keV and Gate-I, respectively, with external uncertainties quoted.

From the data listed in Table 1 it can be derived that for the combined gates Gross 1275 and Gate I (E_γ =1152-1921 keV) the value of $\Delta A/A=(-0.9\pm0.3)*10^{-4}$ and $\Delta A/A=(-0.6\pm0.3)*10^{-4}$, for the two periods, respectively. These values indicate that the overall count rate changes with the values as obtained for the E_γ =169-2451 keV gate, whereas an exchange of count rate between Gross 1275 keV and Gate-I occurs. This exchange may carry information on changes in the partial decay constants if the effect is due to antineutrinos affecting β^+-decay .

The uncertainties in the tabulated values represent statistical uncertainties only. Although statistical uncertainties have greatly benefitted by the long counting periods, the systematic uncertainties have remained unchanged. Hence on the one hand a yet unidentified instrumental effect cannot be excluded to explain the results as presented in Table 1 on the other hand the results are consistent with a physics effect in which the β^+-decay to the ^{22}Ne(1) is hindered by an interaction between antineutrinos and the nucleus ^{22}Na. In that case one expects a reduction in the total decay constant λ, a reduction of the branching ratio of the β^+-decay and a relative enhancement in the EC branching ratio to ^{22}Ne. The reductions show up as negative values of $\Delta A/A$, the enhancement of the EC branching ratio is resulting in a positive value of $\Delta A/A$ for the Gross 1275 keV gate, containing EC-decay events.

In case the effect is purely caused by an antineutrino interaction of antineutrinos with the nucleus ^{22}Na the $\Delta A/A$ value for the 169-2451keV gate at an estimated change in antineutrino flux between reactor-ON and reactor-OFF of $\Delta\varphi=1.0*10^{13}$ cm^{-2}.s^{-1} the cross section becomes $(2.9\pm0.6)*10^{-26}$ cm^2, about twenty orders of magnitude larger than measured for the inverse β-decay process.

Our future work will focus first on a measurement with the same set-up but a β^--source. This source has a very high threshold for β^+-decay and should therefore be sensitive to the unidentified instrumental effect. If the result supports the hypothesis that the present effect is due to an antineutrino interaction with ^{22}Na, we will continue the investigations to identify the properties of the interaction and to find the optimum conditions for antineutrino monitoring of nuclear power reactors.

In October 2014 we started preparations for a measurement series (Koeberg-04) scheduled around the anticipated outage of Unit#1 from February until May 2015.

3 Neutrino Geoscience.

3.1. Introduction.

The long-term scientific goal of the EARTH Foundation is to work towards obtaining a 3D-image of the distribution of radiogenic heat sources in the interior of the Earth by means of antineutrino tomography. Although in the short term the present detector development focuses on reactor monitoring, this long-term goal remains unchanged. On the basis of the rapidly growing geoscience literature on these topics and in the absence of any data, we are exploring the nature of the radiogenic heat sources being either natural radioactive decay, or possibly a natural georeactor. In both cases antineutrinos will be emitted, but a distinction between the two types can be made from their energy spectrum. As indicated in earlier work *(de Meijer and van Westrenen, 2008*) our present knowledge of geoscience cannot rule out georeactors in the core-mantle boundary (CMB) region in the Earth, at depths of approximately 2900 km.

In the previous progress report (EARTH-PRP-10) we described the nuclear explosion model for the formation of the Moon that we developed in a collaboration with with dr V. F. Anisichkin of the Lavrentyev Institute of Hydrodynamics, Siberian Branch of Russian Academy of Sciences, Novosibirsk, Russia. In a joint paper, finally published in Chemical Geology, we re-examined the dynamics of the Earth-Moon system and the energetics of initial Earth-Moon separation. In contrast to previous 'fission' models, our conservative assumption is that the angular momentum of the proto-Earth before Moon formation is close to that of the present-day Earth-Moon system. This is in full agreement with assumptions made in recent three-dimensional hydrodynamic simulations of a giant impact origin for the Moon (*Canup, 2008*). We estimate the amount of energy required to separate the Moon from the Earth in this case and propose nuclear fission as the only known natural process that could supply the missing energy in such a very short time (*de Meijer et al., 2013*).

3.2 Developments

As a next step we have examined various stability-related boundary conditions imposed by a proto-Earth and a Earth-Moon system to comply with basic physics. This work was carried out in a collaboration between the Geoscience Department of the University of Utrecht (dr. Inge Loes ten Kate and BSc student Maarten Reuver) and the VU University Amsterdam - Faculty of Earth and Life Sciences.

The stability of the proto-Earth is manifested by a maximum rotation frequency $\omega_{max} = \frac{L}{I} \leq \sqrt{\gamma \frac{m_{pE}}{a_{pE}^3}}$. In this expression γ is the gravitational constant, m_{pE} indicates the mass of the proto-Earth, an a_{pE} its long axis. At this frequency the centripetal gravitational force and the centrifugal force are equally strong. For a given value L of the angular momentum, ω_{max} is inversely proportional to the moment of inertia of the proto-Earth, I, and hence depends on the shape and the mass distribution of the proto-Earth. First we noticed that the internal gravity-driven differentiation of density in the Earth due to core and crust formation early in its history causes the moment of inertia of the proto-Earth to decrease and consequently speed up its rotation. With increasing oblateness the moment

of inertia increases as well. Angular momentum has a significant effect on the stability of the proto-Earth. Since the rotation frequency depends linearly on the angular momentum of the system, the stability criterion limits the maximum L value. For the proto-Earth we noticed that the system becomes increasing less stable until about L/L_p =2.5, the lower values for the most realistic scenario of a differentiated density as is indicated in Figure 6.

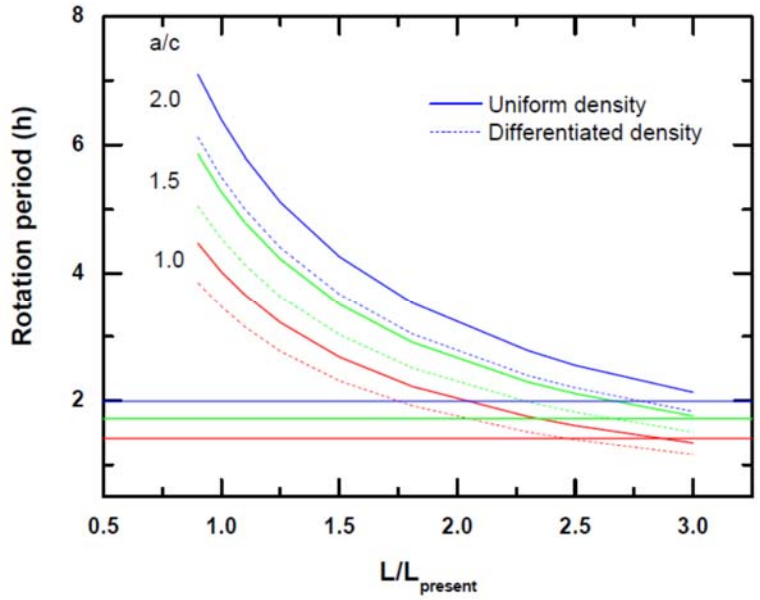

Figure 6. Rotation period as function of angular momentum for uniform and differentiated densities and three values of the oblateness parameter *a/c*.

The study shows that the dynamical stability of the proto-Earth is mainly determined by the differentiation of the density and the oblateness of its shape. In a search for minimal energy of a natural system, the low viscosity of the proto-Earth combined with a high rotation frequency will create an oblate differentiated Earth. With respect to Moon formation, the Giant Impact Model will need a very large angular momentum in the approaches of *Cuk and Stewart, 2012* and *Canup, 2012*, and hence a very "flat" proto-Earth. In our nuclear explosion model *(de Meijer et al., 2013),* much more modest conditions are allowed.

Our present calculations (Reuver *et al.,* 2014) indicate that the proto-Earth in the calculations of Cuk and Stewart (2012) is not dynamically stable and would break-up even before a collision. In the calculations of Canup (2012) the post-collision Earth is rotating too fast for dynamic stability and produces a second moon.

4. References.

Canup, R.M., 2008. Lunar forming collisions with pre-impact rotation. Icarus **196**, 518-538.

Canup, R.M., 2012. Forming a Moon with an Earth-like composition via a giant impact. Science **338**, 1052-1055.

Ćuk, M. Stewart, S.T., 2012. Making the Moon from a fast-spinning Earth: A giant impact followed by resonant despinning. Science **338**, 1047-1052.

de Meijer, R.J., Anisichkin, V.F., van Westrenen, W., 2013. Forming a Moon from terrestrial silicate-rich material. Chemical Geology **345**, 40-49.

de Meijer, R.J. and van Westrenen, W., 2008. The feasibility and implications of nuclear georeactors in Earth's core-mantle boundary region, South African Journal of Science, **104**, 111-118.

de Meijer, R.J., Blaauw, M, and Smit, F.D., 2011. No evidence for antineutrinos significantly influencing exponential β^+ decay, Applied Radiation and Isotopes, **69,** 320-326. doi:10.1016/j.apradiso.2010.08.002..

de Meijer, R.J. and Steyn, S.W., Upper limit on the cross section for reactor antineutrinos changing ^{22}Na decay rates, 2014 Submitted to AstroParticle Physics and ArXiv.org: 1409.6969.

Reuver, M., de Meijer, R.J., ten Kate, I.L. , van Westrenen, W., Boundary conditions for Moon formation, submitted to the Netherlands Journal of Geosciences, special issue on Dutch Planetary Geosciences.